Comparison of NMR Cryoporometry, Mercury Intrusion Porosimetry, and DSC Thermoporosimetry in Characterizing Pore Size Distributions of Compressed Finely Ground Calcium Carbonate Structures

Patrick A. C. Gane,[†] Cathy J. Ridgway,*[,†] Esa Lehtinen,[‡] Rustem Valiullin,[§] Istvan Furó,[§] Joachim Schoelkopf,[†] Hannu Paulapuro,[‡] and John Daicic[||]

Omya Development AG, CH 4665 Oftringen, Switzerland, Helsinki University of Technology, Box 6300, FI-02015 Hut, Finland, KTH Royal Institute of Technology, Teknikringen 30/36, SE-10044 Stockholm, Sweden, and YKI Institute for Surface Chemistry, Box 5607, SE-11486 Stockholm, Sweden

This work investigates for the first time how mercury intrusion porosimetry (MIP), NMR-based cryoporometry, and DSC-based thermoporosimetry compare in revealing the porous characteristics of ground calcium carbonate structures compacted over a range of pressures. The comparison is made using the same source samples throughout. MIP, a much-used method in the characterization of porous structures, has the drawback that the high pressure needed to intrude the mercury may either distort the skeletal porous structure of the sample, especially when compressible materials such as cellulose or binders/latex are present, or lead to a reduction in the measured number of large pores due to the shielding by smaller pores. These effects have previously been addressed using bulk modulus corrections and by modeling the structure permeability to account for the potential shielding. Cryoporometry gives detailed information about the pore size distribution of an imbibition saturated structure. Thermoporosimetry is a relatively new candidate in this field, and it yields both pore size distribution and pore volume. Currently it is somewhat limited in the pore size range detectable, but it is relevant to pigmented coatings. Its potential is identified for capturing the pores involved in the progress of imbibition before saturation is reached.

Introduction

The topic of porous media characterization covers a vast area of research activity. Important porous media parameters include surface free energy and geometry/morphology of the interconnecting pore network. The structural properties that characterize the behavior of a porous substrate, with respect to liquid absorption and permeability, can be broken down using a pore and connecting throat concept primarily into the following: porosity, pore size and size distribution, throat size distribution, connectivity, tortuosity, permeability, and pore/throat shape (including aspect ratio).

While porosity is directly measurable by an adequate porosimetry method, and permeability can be experimentally quantifiable, pore and throat size distributions, connectivity, and, to a certain extent, tortuosity need a more sophisticated description. In particular, to describe throat size distribution, connectivity, and tortuosity requires to date adoption of a simulator program, which constructs a model of discrete pores and throats providing a given connectivity derived from porosimetric data.[1−4] Furthermore, the geometry of the pores and throats is best visualized by using an adequate method of microscopy, among which electron microscopy is widely used, which does go some way toward determining connectivity and tortuosity, at least semiquantitatively. Quantifying connectivity and pore arrangements in space are important issues that still need evaluation when a pore network simulator is involved, as, ideally, it is necessary to reduce the number of ill-defined fitting parameters. Baldwin et al.,[5] using a magnetic resonance imaging technique (MRI) and image analysis, characterized binary pictures in terms of pore morphology and fractal dimensions. Due to the limited resolution of MRI, this analysis is confined to >10 μm pores.

Direct experimental three-dimensional (3D) digitized imaging is in its infancy. For example, microtomography has, as yet, limited resolution (>∼8 μm),[6] just outside the region of micrometers and below the resolution needed for paper coating structures. This, however, is a highly interesting new method, which would allow for an excellent 3D visualization of porous structures and holds much potential for the future.

This paper focuses on methods especially relevant to paper and paper coating structures in particular, to evaluate the pore size distribution. The first method we apply is probably the most accepted means to investigate a porous structure and adopts intrusion/extrusion porosimetry, where the use of mercury as the nonwetting test liquid is the most widespread technique.[7−10] Mercury is an ideal liquid, because it shows a very high contact angle to most solid substrates and, therefore, the Laplace equation can be employed to relate an applied pressure with a relevant pore diameter being intruded by the nonwetting liquid mercury. The main drawbacks of the method are the effects induced by the high pressure applied and the shielding of large pores

* To whom correspondence should be addressed. E-mail: cathy.ridgway@omya.com.
[†] Omya Development AG.
[‡] Helsinki University of Technology.
[§] KTH Royal Institute of Technology.
[||] YKI Institute for Surface Chemistry.

10.1021/ie049448p CCC: $27.50
Published on Web 10/28/2004

by small access throats. It is important to recognize that the pore shielding effect leads to an underestimation of the intrusion volume associated with large pores and an overestimation of the intrusion volume associated with fine pores. To overcome these drawbacks, a number of correction methods are suggested in the literature. The adoption of a correction program, Pore-Comp (Pore-Comp is software developed by the Environmental and Fluid Modelling Group of the University of Plymouth, Devon PL4 8AA, U.K.),[11] described below in the experimental section, provides a way to overcome some of the problems. However, to account for shielding, a model structure from which the shielding is extracted has to be constructed. This is partially artificial and only gives an indication of one of many best-fit pore size distributions. Methods related to mercury porosimetry include water intrusion porosimetry for strongly hydrophobic substrates[12] and liquid extrusion porosimetry, introduced by Miller and Tyomkin,[13] which monitors the extrusion of a wetting fluid from a presaturated structure. Mercury porosimetry was applied to the samples tested in this paper at the Omya Development AG laboratories in Switzerland.

The other two methods, DSC (differential scanning calorimetry) thermoporosimetry (measured at the Helsinki University of Technology) and NMR (nuclear magnetic resonance) cryoporometry (measured at the Royal Institute of Technology, Stockholm, Sweden) have a lot of common elements despite their misleadingly different names of convention. Both methods are based on the decrease in the melting temperature of a liquid when confined in small pores or capillaries. Because of the presence of supercooling, both methods usually approach the problem in reverse and detect the suppression of melting which is a consequence of the effect of local curvature on the equilibrium state of the probe liquid; the same reasoning lies behind the size effect well-known to influence vapor pressure. Finally, both methods assume, as verified for pores larger than a few nanometers, that the solid−liquid surface energy, the density of frozen probe liquid and the enthalpy of fusion are the same in the pores as in the bulk. The difference lies in the mode of detection.

DSC thermoporosimetry observes heat transfer in a measurement consisting of dynamic and isothermal steps, from which the amount of a liquid molten within a given temperature range can be calculated with the help of the known enthalpy of fusion. In contrast, NMR cryoporometry does not detect the actual melting of a probe liquid and the temperature range over which this happens but instead records the fractions of frozen and unfrozen liquid as a function of temperature. This is achieved through the dramatically different nuclear spin relaxation times of molecules in liquid and solid states, which allows the NMR signal from these two compartments/states to be clearly distinguished. These different detection pathways may lead to different size resolutions and detection limits for DSC and NMR. Note that both methods have been successfully introduced to analyze paper-related structures: DSC thermoporosimetry by Maloney and Paulapuro[14] to study papermaking fiber wall structures, and NMR cryoporometry by Furó and Daicic[15] to analyze paper coating structures.

Several different porometric methods have already been compared, typically pairwise, by others.[14,16−20] Those comparisons were usually performed in model systems, typically porous glasses prepared by liquid−liquid phase separation procedures. Ours is the first attempt to compare three independent porometric methods on an industrially relevant material that, moreover, was produced by compression. With this paper we make a first approach at a direct comparison among the three different methods. We start with a series of samples that have some importance in the paper coating industry. The samples consist of mineral pigment, namely fine ground $CaCO_3$, in the form of compressed porous tablet structures. These structures have been analyzed previously in detail for their pore structure including by mercury porosimetry and experimental absorption together with pore network modeling, and comparisons were made with experiment using a Bosanquet-based wetting algorithm applied to the model structures.[4,21]

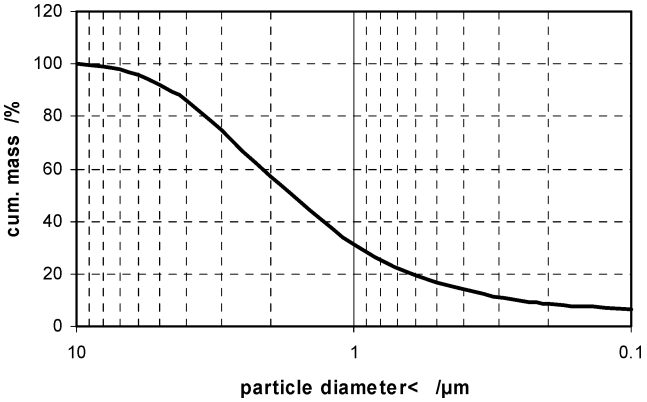

Figure 1. Particle size distribution of the powder used for consolidation of porous tablets expressed as cumulative mass percent less than an equivalent Stokesian diameter.

The objective of capturing the absorption dynamic in real time by freezing prior to saturation will in the future be the basis for developing the thermoporometric method further in order to establish the validity or otherwise of the preferred pathway dynamics predicted by Schoelkopf et al.,[22] which were derived from the structure and absorption modeling. Future work will also involve coarser standardized structures to understand better the relative advantages and limitations of each method.

Materials

A commercially available polyacrylate dispersant treated dry powder product was chosen, Hydrocarb 60 OG from Omya AG, derived from natural $CaCO_3$, which is produced by wet grinding from limestone (Orgon, France) and subsequent spray drying. The cumulative particle size distribution curve of the material, as measured by sedimentation (measurements made on a Sedigraph 5100 from Micromeritics Instrument Corp., Norcross, GA), is shown in Figure 1.

The powder was compacted in a steel die at different compaction pressures applied by an hydraulic press to form macroscopic tablets with a diameter of 46 mm and a typical thickness of approximately 18 mm. The tablets did not contain any binders or additives. Details of this method are described in the literature.[23,24] The range of applied press forces, F, the press area, A, and the resulting pressures, P, are listed in Table 1.

Using this sample formation technique, a wide range of porosities and mean pore diameters could be achieved. A similar range of such structures was previously used for consistent studies of liquid imbibition and permeation,[4] without changing the surface chemistry or

Table 1. Conversion Table of Applied Forces to Resulting Pressures [Cross-Sectional Area A = 17.35 cm^2 (±0.16)]

applied force F/kN (±5)	effective pressure P/MPa (±2.7)	applied force F/kN (±5)	effective pressure P/MPa (±2.7)
100	57.6	400	230.6
200	115.3	450	259.4
300	172.9		

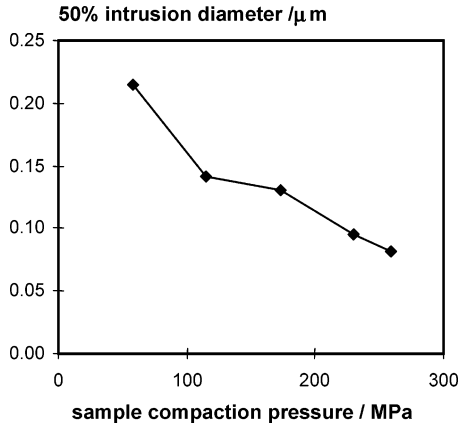

Figure 2. Experimental 50% mercury intrusion volume data showing that the d_{50} pore diameter (and porosity) decreases as a function of increasing sample formation pressure.

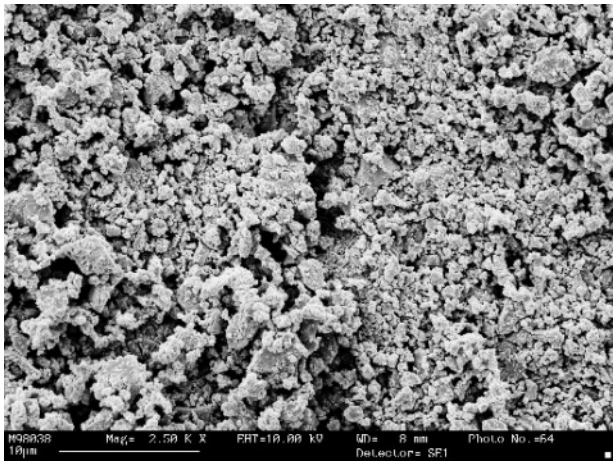

Figure 3. SEM image of surface of tablet made under compaction pressure of 57.6 MPa.

intrinsic pore geometry. Figure 2 shows that the intrusion diameter is not necessarily a smooth function of sample compaction pressure. It is on this basis that the following analyses were made considering experimental porosity as the independent variable and not external sample compression.

A range of tablets characterized according to porosity was thus selected and each tablet was cut into four pieces, providing to each of the involved laboratories one piece of a tablet that could be further subdivided for the respective porosimetric analyses.[4] The uniformity of the tablet structures was also tested and found to be very reproducible.[3,25−27] An SEM picture of the cross section of one of the tablets made under the compaction pressure of 57.6 MPa is shown in Figure 3.

Methods

Mercury Porosimetry. Mercury is a nonwetting fluid and thus will not penetrate pores by capillary action but will do so by applying an external pressure. Mercury porosimetry measures the intruded volume in relation to the mass of the sample at a specific pressure; this pressure can then be converted to an equivalent Laplace diameter if required, and the cumulative curve of intruded volume per unit mass of sample into such diameters greater than a given value forms the usual representation of the data. It may also be represented as the logarithm of the differential intrusion volume so as to form a distribution of effective pore size. The areas under the peak of this type of curve are significant in that they equal the pore volumes of each Laplace pore size fraction. These curves also show more clearly the regions of the intrusion curve with a steeper intrusion-pressure gradient.

Mercury intrusion measurements were made using a Micromeritics Autopore III mercury porosimeter. The maximum applied pressure of mercury was 414 MPa, equivalent to a Laplace throat diameter of 0.004 μm (4 nm). The equilibration time at each of the increasing applied pressures of mercury was set to 60 s, and a sample mass of approximately 1.5 g was used. The mercury intrusion measurements were corrected, using the software Pore-Comp, for the compression of mercury, expansion of the penetrometer, and compressibility of the solid phase of the sample. The following equation from Gane et al.[11] was used:

$$V_{\text{int}} = V_{\text{obs}} - \delta V_{\text{blank}} + \left[0.175(V^1_{\text{bulk}}) \log\left(1 + \frac{P}{1820}\right)\right] - V^1_{\text{bulk}}(1 - \Phi^1)\left(1 - \exp\left[\frac{P^1 - P}{M_{\text{ss}}}\right]\right) \quad (1)$$

in which V_{int} is the volume of intrusion into the sample, V_{obs} the intruded mercury volume reading, δV_{blank} the change in the blank run volume reading, V^1_{bulk} the sample bulk volume at atmospheric pressure, P the applied pressure, Φ^1 the porosity at atmospheric pressure, P^1 the atmospheric pressure, and M_{ss} the bulk modulus of the solid sample.

The pressure, P, required to intrude mercury into a capillary of diameter, d, is given by the Laplace equation

$$d = \frac{-4\gamma_{\text{LV}} \cos\theta}{P} \quad (2)$$

where γ_{LV} (=0.485 N m^{-1}) is the mercury liquid−vapor surface tension, and θ is the contact angle the liquid mercury makes with the solid surface (=140° in this study).

DSC Thermoporosimetry. The measurement is based on the decrease in the melting or freezing temperature of a liquid confined within small pores or capillaries. The following form of the Gibbs−Thomson equation shows the relationship between melting temperature and pore size when the pores are assumed to be cylindrical:

$$d = \frac{-4V_{\text{m}}\gamma_{\text{LS}}}{\Delta H_{\text{m}}(T_0 - T_d)} \quad (3)$$

where d is the cylindrical pore diameter, V_{m} the molar volume of frozen probe, γ_{LS} the surface energy of the solid−liquid interface of the probe, ΔH_{m} the latent heat of melting of the probe, T_d the melting temperature of the probe liquid corresponding to pore diameter d, and

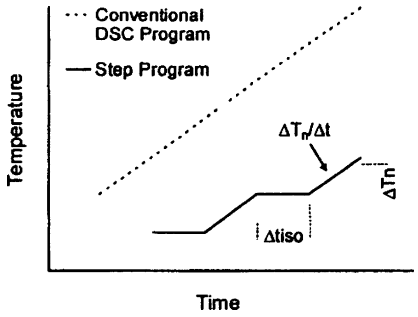

Figure 4. Principle of stepwise measurement of melting heat.[28]

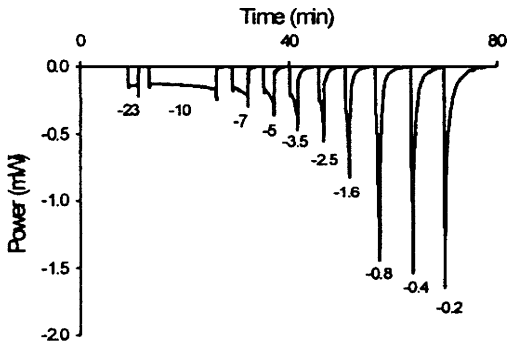

Figure 5. Temperature program used in porosity measurement of fibers with water.[14,28]

T_0 the melting point of the bulk probe liquid at normal pressure. A more detailed description of this procedure is given by Maloney and Paulapuro.[14]

The probe liquid used in the porosity measurements was cyclohexane. Earlier studies[23] have shown that these carbonate structures are completely wetted and saturated by organic liquids with a surface tension $\lesssim$50 mN m^{-1}. Unlike the case of oil-saturated structures exposed to water, the previously unwetted samples do not disintegrate when exposed to cyclohexane alone. Its normal melting point, 6.54 °C, was used for the value of T_0 in these measurements. The smallest measurable pore size is about 5 nm, because smaller pores than this contain only nonfreezing cyclohexane, dependent on <1 nm constriction effects. The plateau in sensitivity of the melting temperature of cyclohexane to curvature change dictates the practical upper limit for the size of the measurable pores, in that the experimental upper limit is primarily set by either the differential thermal step size in the DSC or the applied temperature gradient in NMR.

A measurement run is carried out by first lowering the temperature enough to freeze all freezable probe liquid. Then the temperature is raised according to the chosen temperature program. An essential feature of our application of thermoporosimetry is the stepwise change in temperature. Each temperature step corresponds to a step in pore diameter according to the Gibbs−Thomson equation. The volume of molten liquid is calculated from the energy consumption in a step. An example of the step temperature program and the resulting endotherm are shown in Figures 4 and 5, respectively, for water-saturated pulp fibers. For a typical cyclohexane-saturated coating, the temperature range is from −4.8 to +6.3 °C with the corresponding Gibbs−Thomson pore diameter range being from 10 to 500 nm. This is sufficient to cover the entire pore size range for most coating samples.

Calorimetric measurements were made using a Mettler Toledo DSC821 differential scanning calorimeter (DSC). The calorimeter was calibrated using measurements of standards, which include known isothermal sections.

During the first measurements of the experimental samples, an artifact was discovered. It was found to be caused by the capillarity of the closed DSC crucible itself, most probably due to the joint between the bottom of the crucible and the lid, resulting in an overestimation of the pore-bound liquid. This effect was verified with dummies, i.e., by putting pieces of aluminum with roughly the same size and shape as pigment specimens into the crucible. The magnitude of the artifact was shown to be about 0.45 μL, while the pore volumes of the pigment specimens themselves were independently determined to be about 2−2.5 μL (14−15 mg samples). The effect of this artifact was therefore eliminated by subtraction of the blank run from the experimental data, and this is reflected in the results reported here.

A further potential for error, caused by the capillarity between the pigment specimen and crucible bottom, was shown to have only a marginal effect, and no correction procedure was undertaken.

NMR Cryoporometry. NMR cryporometry[16,20] is, like DSC thermoporosimetry, based on the suppression of melting/freezing point in confined liquids as described by the Gibbs−Thomson equation (eq 3). In contrast to DSC, one does not detect the actual melting as manifested by heat transfer but instead measures the fraction of liquid molten at any particular temperature. This measurement is performed by the spin−echo pulse sequence[29,30] with appropriate echo times (10 ms in the current experiments). The spin−echo NMR experiment keeps the NMR signal from those nuclei that reside in mobile molecules because their magnetization does not relax to zero under the selected echo time. On the other hand, the NMR signal from nuclei that reside in immobile molecules is effectively canceled because the (transverse) spin relaxation rate of those nuclei is large and thereby their magnetization relaxes to zero during the set echo time.

Hence, the commonest NMR cryoporometric experiment is rather simple: one first lowers the temperature so that all liquid in the investigated porous system freezes as verified by the lack of spin−echo NMR signal. Then, the temperature is stepwise increased and at each new temperature a new spin−echo experiment is performed. As liquid confined to larger and larger pores melts, one detects a spin−echo NMR intensity that increases with increasing temperature as illustrated in Figure 6. The derivative of the acquired temperature−intensity curve provides, after appropriate scaling,[31] the pore size distribution as provided in Figure 10. Similarly to the DSC measurements, cyclohexane was used in the present experiments, with properties and limitations as provided above. All ^{1}H NMR experiments were performed in a Bruker DMX200 spectrometer equipped with a conventional 10 mm high-resolution NMR probe. The temperature was controlled by a Bruker BVT3000 unit with 0.1 K temperature resolution and <0.05 K temperature stability.

Results

The mercury porosimetry curves for the five sample tablets are shown in Figure 7. Porosities were calculated using the corrected total intrusion volume as calculated

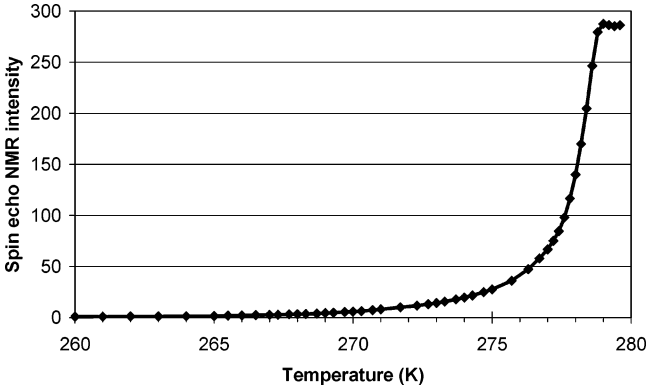

Figure 6. Spin−echo NMR intensity (arbitrary units) with respect to temperature. Data from the 28.72% porosity sample.

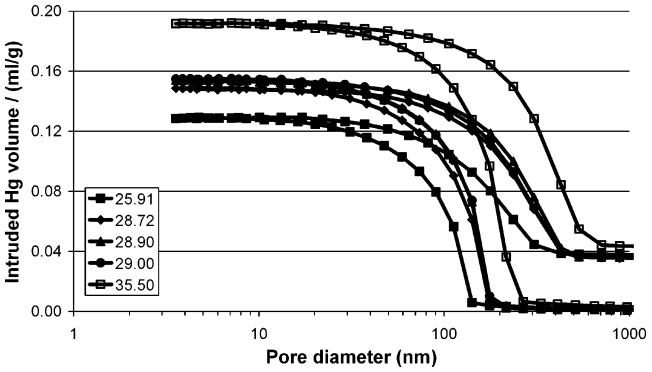

Figure 7. Mercury intrusion porosimetry curves of the range of porous tablets. Samples are indicated by their porosity values (ϕ%). The intrusion volume per gram of sample is plotted against the Laplace equivalent capillary diameter.

from eq 1, having determined the sample volume and skeletal volume. The curves are then plotted with the labels corresponding to their porosities. The differences between the intrusion and extrusion curves show that there is hysteresis behavior as would be expected due, at least partly, to the pore shielding effect.

These corrected intrusion data indicate that the distribution of intrusion pressures is smooth and the curves are continuous. This reflects the relatively broad particle size distribution of the ground calcium carbonate and hence the highly connected continuity of the pore network. Pore shielding, due to the need to force the nonwetting mercury to break through fine connecting features between larger pores (throats), if present, will conspire to underestimate the volume associated with the large pores and simultaneously overestimate the intrusion volume of the fine ones in this display of Laplace diameters (Figure 7). The plateau nature of the cumulative intrusion indicates that this methodology is able to probe all the existing pore sizes present in such coating pigment structures, with all the samples containing Laplace equivalent pore sizes $\geq$10 nm. A typical pore size of ~100 nm is commonly found in paper coating structures, with pores as large as ~500 nm being found in matte paper coatings. The excellent reproducibility of the sample preparation and the mercury intrusion porosimetry technique is demonstrated by the two independent sample curves relating to the tablets with 28.9% and 29.0% porosity, respectively. The data lie directly superimposed.

Using these tablets consisting of the same skeletal material provides a uniform gradation of pore network structure as a function of porosity/compression. This is

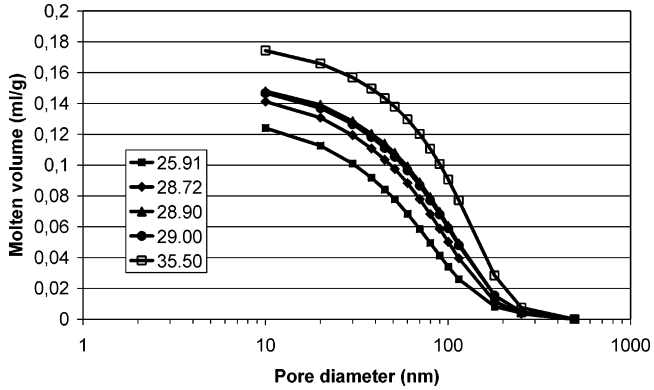

Figure 8. Molten pore liquid volume curves from DSC thermoporosimetry. Samples are indicated as in Figure 6. The volume of the molten liquid is plotted against the Gibbs−Thomson equivalent capillary diameter.

seen by the monotonic logarithmic relationship of the intrusion curves to one another. As porosity increases, so does the intrusion volume across the whole range of pore sizes. Given the logarithmic scale of pore sizes, this indicates that the structure is compressing across an approximately log-linear structure factor distribution. The structures are therefore mathematically similar and could in principle be defined according to a fractal scaling across the range of study.

The corresponding results from DSC thermoporosimetry are shown in Figure 8 covering the equivalent Gibbs−Thomson pore diameter range of 10−500 nm. They are from an ongoing work for developing the method appropriate for measuring the porosities of pigment structures and pigment coatings on paper. The molten pore liquid volume of each step was calculated using the heat consumed in each step as the starting point. The curves were obtained by summing the molten volumes of each step and then plotting the cumulative molten pore liquid volume curves. Nonfreezing pore liquid contribution is not included, as it is not possible to distribute it over the measured pore size range on the basis of these measurements. However, the total nonfreezing pore liquid amount, determined from the difference between the known uptake and the thermal capacity plus latent heat of the melted quantity, varied between about 0.015 and 0.020 mL/g depending on the sample.

Much of what has been said about mercury porosimetry results also applies here. The cumulative curves are smooth but show a more gradual transition toward plateaus at small pore sizes. The shielding effect in mercury porosimetry might at least partially account for an overestimation of pores approaching the plateau and so accentuating the pore size cutoff effect. The start of the growth of the curves is initially smoother than in mercury porosimetry measurements, indicative of a potential breakthrough pressure in the mercury intrusion measurement. In all, DSC thermoporosimetry seems to give a wider pore size distribution than mercury porosimetry, as can also be seen from Figures 9 and 11, although most probably overestimating the volume contribution of the smallest pores.

DSC thermoporosimetry puts the samples in almost the same order as mercury porosimetry, and also the spacing of the curves is quite similar. Only the curves corresponding to 28.90% and 29.00% porosity have changed their relative places, but actually they remain almost superimposed as before. The indicated total pore

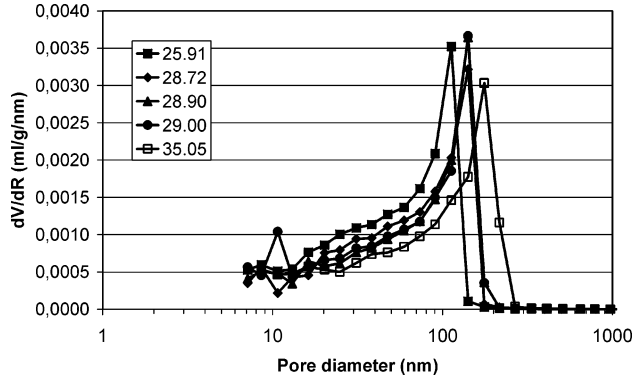

Figure 9. Pore size distribution (PSD) curves of the range of porous tablets from mercury intrusion porosimetry measurements. Samples are indicated as in Figure 6. The increase of intruded volume divided by the change of corresponding capillary radius is plotted against the Laplace equivalent capillary diameter.

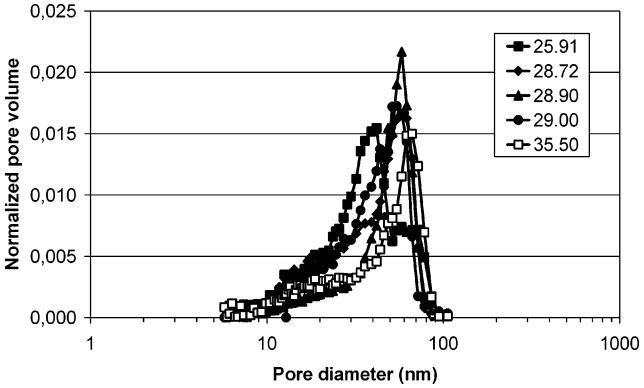

Figure 10. Normalized pore size distribution (PSD) from NMR cryoporometry. Normalization is made over the total integral under each curve being set equal to 1.

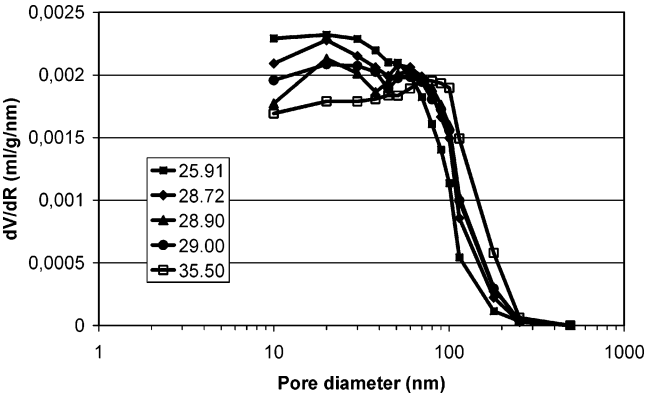

Figure 11. Pore size distribution (PSD) from thermoporosimetry. Samples are indicated as in Figure 6. The volume increase of molten pore liquid divided by the change of corresponding capillary radius is plotted against the Gibbs−Thomson equivalent capillary diameter.

volumes are a little smaller than from mercury porosimetry. This is natural as DSC thermoporosimetry results do not include the volume of nonfreezing (never frozen) pore liquid.

Figures 9−11 show pore size distributions (PSD) for the three methods as dV/dR curves, where dV means volume increase of a measuring step and dR refers to the corresponding change in pore radius over that step. Mercury porosimetry (Figure 9) gives three locations of the maximum, of which the middle one corresponds to the maxima of the middle three porosity curves, at three consecutive measuring points between 100 and 200 nm pore diameters.

Figure 10 shows the pore size distributions from NMR cryoporometry measurements. The curves have been normalized to give the total integration area of unity. The locations of the maxima are at smaller pore diameters than the locations of maxima of the mercury porosimetry curves. The range of the located maxima from NMR is 40−70 nm. Although the NMR data can in principle be collected in an absolute way by comparing the sample measured signal to that of an independent (external to the sample, but within the NMR probe) reference, the present method did not include such a reference and therefore recorded only the relative variation of the signal. Hence, data are not available for constructing corresponding plots for absolute pore size−volume distributions from the NMR experiments. However, this is not of importance when it is realized that the imbibition processes and, thereby, the amount of total imbibed liquid [in millimeters per gram (mL/g)] were identical for the DSC and NMR experiments; i.e., the total amount of imbibed cyclohexane is the same in the DSC and the NMR measurements per unit mass of sample of given porosity. In both methods the porous samples were immersed in cyclohexane, then removed once the cyclohexane had imbibed (virtually spontaneously), and then the measurements were made. Thus, the scaling for the DSC method can be used directly to scale the data for the NMR method on a per mass basis for each corresponding sample.

If the NMR method were being used alone, the total imbibed amount could have been obtained by simply measuring the mass before and after immersion. That simple mass measurement would simultaneously fix the quantitative scale for Figure 7 if needed and, hence, any hypothetical corresponding NMR curve where the latter could be obtained by stepwise integrating the PSD in Figure 9 and adjusting the scale so the cumulative amount gives the mL/g value which is set by the mass of imbibed cyclohexane. [The DSC calculation does not actually calculate the mL/g scale in this way, but rather from (heat transfer)/(cyclohexane melting enthalpy). However, it too could be determined this same way using simple mass balance.]

The PSD curves from DSC thermoporosimetry are quite different. They do not decrease toward zero at small pore diameters after the initial increase as do the PSD curves from mercury porosimetry and NMR measurements, but instead, depending on the curve, more or less level out. This is a consequence of what can be seen in Figure 8; i.e., the potential overestimation of the volume of the smallest pores is in effect similar to that shown by mercury porosimetry, but even greater for the NMR thermal analysis. Nonetheless, if the cumulative curves are extrapolated, the trend is clearly once again downward for the pore size distribution at the level of the finest pores. The relative order of curves has been reproduced, and follows those as seen using mercury porosimetry (Figure 10).

Work is still needed to find out why DSC obviously overestimates the volume contribution of the smallest pores compared with the other two methods. One explanation for the smaller pore radii found by the two thermoporometric methods possibly derives from the fact that they are both based on imbibition saturation. Following the findings of Schoelkopf et al.,[27] it is found that the liquid permeabilities of imbibition saturated structures of the very same pigment tablets as those

used in this paper were lower than expected at low differential pressures. This was explained by the presence of entrapped air. This finding in turn confirmed a theory proposed earlier by these authors describing preferential imbibition into pores with a size optimum, given in their case by the Bosanquet equation or, more precisely, with a certain radius/length aspect ratio as discussed by Sorbie et al.[32] and determined by Ridgway et al.[33] This can be visualized by considering a network of low aspect ratio fine pores, remembering that generally a fine pore in our structures is equally as short as its diameter, i.e., too short to establish viscous drag while filling, in combination with enough reservoir volume between them, such that a preferred pathway of invasive imbibition into these fine pores can occur. It was also shown, using the Pore-Cor computer network simulator (Pore-Cor is software developed by the Environmental and Fluid Modelling Group of the University of Plymouth, Devon PL4 8AA, U.K.), that ganglia controlled by larger pores are bypassed or at least the access to them is limited.[22] The consequence is that these "slow pathways" may remain with entrapped microbubbles of air or vapor which may dissolve in polar liquids but do not dissolve in the alkanes used in the reported experiments. The entrapped bubbles, occurring preferentially in larger pores, restrict flow and therefore decrease permeability unless they are compressed or displaced by high differential pressures. For the imbibition saturated samples used in the thermoporometric methods, this model will apply and would explain the observed shift toward smaller pore sizes when compared to mercury porosimetry, in which all relevant pores are eventually intruded.

Conclusions

Three methods, mercury intrusion porosimetry (MIP), NMR cryoporometry, and DSC thermoporosimetry, have been compared in this work for the first time using broad size distribution materials based on industrial samples consisting of calcium carbonate tablets compacted to five different porosity levels. The sampling was completely consistent in that the same samples were used in all three measurement systems. The comparisons between the three methods were performed by observing the respective reported pore volume of the samples, taken within a relevant pore diameter range, together with the respective pore size distributions that the three methods gave.

For absolute pore volume comparisons, data were available only from MIP and DSC thermoporosimetry. These methods place the samples in nearly the same mutual order with very similar spacing of the cumulative pore volume curves. The indicated total pore volumes are nearly the same, with MIP giving slightly higher values.

Pore size distributions (PSD) were determined as dV/dR curves, i.e., the change of pore volume with respect to the change of pore radius. The maxima of the PSD curves were in the neighborhood of 100 nm pore diameter with MIP and NMR cryoporometry. The maxima of the former were somewhat above those for the NMR; i.e., MIP maxima were between 100 and 200 nm, while the maxima of the NMR were below 100 nm. An explanation for this could be air bubbles in larger pores, which restrict flow into these during imbibition of the saturating liquid and shift the PSD toward smaller pores.

No such maxima in the PSD curves could be obtained with DSC thermoporosimetry, but only a leveling out of the curves at approximately the same pore diameter range where the maxima of NMR cryoporometry occurred. This gives also an overestimation of the pore volume at the smallest pore diameters. The reasons for this will need further examination, but the trend clearly showed also the expected potential leveling of the cumulative curves. One approach could be to use a model for the pore structure to account for the shielding effect of MIP[11] and then to compare this model with the distributions obtained by the saturated liquid methods of both DSC and NMR derived directly without the mercury shielding correction.

It should be noted that previous comparisons of porometric methods[14,16−20] typically provided very similar pore size distributions. Some of the compared methods were the same as the ones here (such as MIP and DSC). Clearly, our results contradict those findings. As a possible underlying reason, those earlier experiments were usually performed in porous glasses and silicas with typically lower pore sizes. Smaller pores and thereby larger changes in melting points may mask some artifacts of thermo- and cryoporometric methods. On the other hand, porous glass structures have high interconnectivity and a slowly varying wall curvature while the samples investigated here have a range of skeletal particle/element sizes resulting in highly discontinuous geometries. If anything, our results command that caution be applied when interpreting porometric data for and above ~100 nm pore sizes and in materials deviating from idealized model systems.

Literature Cited

(1) Matthews, G. P.; Moss, A. K.; Ridgway, C. J. The Effects of Correlated Networks on Mercury Intrusion Simulations and Permeabilities of Sandstone and Other Porous Media. *Powder Technol.* **1995**, *83*, 61.

(2) Matthews, G. P.; Ridgway, C. J.; Spearing, M. C. Void Space Modeling of Mercury Intrusion Hysteresis in Sandstone, Paper Coating, and Other Porous Media. *J. Colloid Interface Sci.* **1995**, *171*, 8.

(3) Ridgway, C. J.; Schoelkopf, J.; Matthews, G. P.; Gane, P. A. C.; James, P. W. The Effects of Void Geometry and Contact Angle on the Absorption of Liquids into Porous Calcium Carbonate Structures. *J. Colloid Interface Sci.* **2001**, *239*, 417.

(4) Schoelkopf, J.; Ridgway, C. J.; Gane, P. A. C.; Matthews, G. P.; Spielmann, D. C. Measurement and Network Modeling of Liquid Permeation into Compacted Mineral Blocks. *J. Colloid Interface Sci.* **2000**, *227*, 119.

(5) Baldwin, C. A.; Sederman, A. J.; Mantle, M. D.; Alexander, P.; Gladden, L. F. Determination and Characterization of the Structure of a Pore Space From 3D Volume Images. *J. Colloid Interface Sci.* **1996**, *181*, 79.

(6) Goel, A.; Tzanakakis, M.; Huang, S.; Ramaswamy, S.; Choi, D.; Ramarao, B. V. Characterization of the Three-Dimensional Structure of Paper Using X-ray Microtomography. *Tappi J.* **2001**, *84*, 1.

(7) Abrams, L.; Favorite, C. W.; Capano, P. J.; Johnson, R. W. Using Mercury Porosimetry to Characterize Coating Pore Structure and Its Relation to Coating Optical Performance. *Coat. Conf.* **1996**, 185.

(8) Johnson, R. W.; Abrams, L.; Maynard, R. B.; Amick, T. J. Use of Mercury Porosimetry to Characterize Pore Structure and Model End-Use Properties of Coated Papers—Part I: Optical and Strength Properties. *Tappi J.* **1999**, *82*, 239.

(9) Larrondo, L.; St. Amour, S. The Porous Structure of Paper Coatings—a Comparison of Mercury Porosimetry and Staini...Bition Methods of Measurement. *TAPPI Coat. Conf.* **1995**, 79.

(10) Bodurtha, P. A.; Matthews, G. P.; Kettle, J. P.; Lohmander, S.; James, P. W. The influence of structural anisotropy on fluid

permeation in porous media. *2001 Advanced Coating Fundamentals Symposium Proceedings, San Diego*; Tappi Press: Atlanta, 2001; p 393.

(11) Gane, P. A. C.; Kettle, J. P.; Matthews, G. P.; Ridgway, C. J. Void Space Structure of Compressible Polymer Spheres and Consolidated Calcium Carbonate Paper-Coating Formulations. *Ind. Eng. Chem. Res.* **1996**, *35*, 1753.

(12) Fadeev, A. Y.; Eroshenko, V. A. Study of Penetration of Water into Hydrophobized Porous Silicas. *J. Colloid Interface Sci.* **1997**, 275.

(13) Miller, B.; Tyomkin, I. Liquid Porosimetry: New Methodology and Applications. *J. Colloid Interface Sci.* **1994**, *162*, 163.

(14) Maloney, T.; Paulapuro, H. Themoporosimetry of Pulp Fibers. *Twelfth Fundamental Research Symposium, Oxford*; The Pulp and Paper Fundamental Research Society: Lancashire, U.K., 2001; p 897.

(15) Furo, I.; Daicic, J. NMR Cryoporometry: A Novel Method for the Investigation of the Pore Structure of Paper and Paper Coatings. *Nordic Pulp Pap. Res. J.* **1999**, *14*, 221.

(16) Overloop, K.; Van Gerven, L. Freezing Phenomena in Absorbed Water As Studied by NMR. *J. Magn. Reson., A* **1993**, *101*, 179.

(17) Ishikiriyama, K.; Todoki, M.; Min, K. H.; Yonemori, S.; Noshiro, M. Thermoporosimetry—Pore Size Distribution Measurements for Microporous Glass Using Differential Scanning Calorimetry. *J. Therm. Anal.* **1996**, *46*, 1177.

(18) Hansen, E. W.; Simon, C.; Hausgrud, R.; Raeder, H.; Bredesen, R. Probing Pore Size Distributions by Cryogenic- and Relaxation 2H-NMR. *J. Phys. Chem. B* **2002**, *106*, 12396.

(19) Rigby, S. P.; Fletcher, R. S.; Raistrick, J. H.; Riley, S. N. Characterisation of Porous Solids Using a Synergistic Combination of Nitrogen Sorption, Mercury Porosimetry, Electron Microscopy and Micro-Porous X-ray Imaging Techniques. *Phys. Chem. Chem. Phys.* **2002**, *4*, 3467.

(20) Strange, J. H.; Rahman, M.; Smith, E. G. Characterization of Porous Solids by NMR. *Phys. Rev. Lett.* **1993**, *71*, 3589.

(21) Bosanquet, C. H. On the Flow of Liquids into Capillary Tubes. *Philos. Mag., Ser. 6* **1923**, *45*, 525.

(22) Schoelkopf, J.; Gane, P. A. C.; Ridgway, C. J.; Matthews, G. P. Influence of Inertia on Liquid Absorption into Paper Coating Structures. *Nordic Pulp Pap. Res. J.* **2000**, *15*, 422.

(23) Gane, P. A. C.; Schoelkopf, J.; Spielmann, D. C.; Matthews, G. P.; Ridgway, C. J. Fluid Transport into Porous Coating Structures: Some Novel Findings. *Tappi J.* **2000**, *83*, 77.

(24) Schoelkopf, J. Observation and Modelling of Fluid Transport into Porous Paper Coating Structures. Ph.D. Thesis, University of Plymouth, U.K., 2002.

(25) Schoelkopf, J.; Gane, P. A. C.; Ridgway, C. J.; Spielmann, D. C.; Matthews, G. P. Rate of vehicle removal from offset inks: a gravimetric determination of the imbibition behaviour of pigmented coating structures. *Tappi 2001 Advanced Coating Fundamentals Symposium Proceedings, San Diego*; Tappi: Atlanta, 2001; p 1.

(26) Schoelkopf, J.; Gane, P. A. C.; Ridgway, C. J. Practical observation of deviation from Lucas-Washburn scaling in porous media. *TRI/Princeton International Workshop, Princeton*; 2001.

(27) Schoelkopf, J.; Gane, P. A. C.; Ridgway, C. J. Observed Non-Linearity of Darcy Permeability in Compacted Fine Pigment Structures. *Colloids Surf. A: Physicochem. Eng. Aspects* **2004**, *236*, 111.

(28) Maloney, T. C. Thermoporosimetry by isothermal step melting. *Pre-symposium of the 10th ISWPC—Recent Advances in Paper Science and Technology, Korea TAPPI, Seoul*; Tappi Press: Atlanta, 1999; p 245.

(29) Carr, H. Y.; Purcell, E. M. Effects of Diffusion on Free Precession in Nuclear Magnetic Resonance Experiments. *Phys. Rev.* **1954**, *94*, 630.

(30) Hahn, E. L. Spin Echoes. *Phys. Rev.* **1950**, *80*, 580.

(31) Valiullin, R.; Furo, I. Low-Temperature Phase Separation of a Binary Liquid Mixture in Porous Materials Studied by Cryoporometry and Pulse-Field-Gradient NMR. *Phys. Rev. E* **2002**, *66*.

(32) Sorbie, K. S.; Wu, Y. Z.; McDougall, S. R. The Extended Washburn Equation and Its Application to the Oil/Water Pore Doublet Problem. *J. Colloid Interface Sci.* **1995**, *174*, 289.

(33) Ridgway, C. J.; Gane, P. A. C.; Schoelkopf, J. Effect of Capillary Element Aspect Ratio on the Dynamic Imbibition With Porous Networks. *J. Colloid Interface Sci.* **2002**, *252*, 373.

Received for review June 24, 2004
Revised manuscript received September 10, 2004
Accepted September 10, 2004

IE049448P